strain release can be explained in two ways. High fluid pressures can both reduce V_P (*20*) and cause stable sliding by reducing the effective normal stress on the fault (*21*). This process is probable at Parkfield where a few lines of evidence suggest the fluid pressures are high under Middle Mountain (*22*). If the low V_P rocks exhibit stable sliding, then the locked zone may be smaller where such rocks are present to greater depths; in this case the amount of strain that can be stored in that area would be reduced (*23*). Thus in those areas where stable sliding is present to unusual depths, the fault may not be able to store enough strain to produce large earthquakes. This notion could account for the limits on the rupture of the Loma Prieta earthquake and why little moment was released near the hypocenters of the Morgan Hill and Parkfield earthquakes.

Another possibility is that the areas with high displacement in the geodetic and seismic-waveform models actually represent areas where the stress drop is high and that the true slip pattern covers a wider area. This scenario is possible because in these models a uniform rigidity is used to convert the observed stress drop to slip. Thus a larger area may slip during the mainshock, but the geodetic and waveform observations are primarily sensitive to the areas of the fault that have a high rigidity and high V_p (*24*). In either case a dynamic rupture might end when it attempts to propagate through a region of low V_P.

If the material properties of the fault zone and the surrounding rocks control the manner in which the fault produces earthquakes, then V_P models could be used in earthquake prediction. For instance, current long-term prediction methods rely on our ability to identify fault segments that will fail in individual large earthquakes (*25*). Identification of fault segments has been based on surface geology, historic seismicity, and microseismicity (*13, 25, 26*); however, such observations are not always available or definitive. The use of V_P models to augment these techniques may help to identify segment boundaries. Proper fault segmentation and identification of the parts of a fault segment likely to release the most moment could also allow improved prediction of strong ground motions.

REFERENCES AND NOTES

1. C. R. Allen, *Stanford Univ. Publ. Geol. Sci.* **11**, 70 (1968).
2. D. Eberhart-Phillips, *J. Geophys. Res.* **94**, 15,565 (1989); *ibid.* **95**, 15,343 (1990).
3. A. J. Michael, *Bull. Seismol. Soc. Am.* **78**, 1199 (1988).
4. D. Eberhart-Phillips, V. F. Labson, W. D. Stanley, A. J. Michael, B. D. Rodriguez, *Geophys. Res. Lett.* **17**, 1235 (1990).
5. C. H. Thurber, thesis, Massachusetts Institute of Technology (1988).
6. J. Um and C. H. Thurber, *Bull. Seismol. Soc. Am.* **77**, 972 (1987).
7. W. H. Bakun and T. V. McEvilly, *J. Geophys. Res.* **89**, 3051 (1984); W. H. Bakun and A. G. Lindh, *Science* **229**, 619 (1985); U.S. Geological Survey Staff, *ibid.* **247**, 286 (1990).
8. M. Matsu'ura, D. D. Jackson, A. Cheng, *J. Geophys. Res.* **91**, 12,661 (1984); W. H. Prescott, M. Lisowski, J. C. Savage, *ibid.* **86**, 10,853 (1981).
9. C. M. Wentworth and M. D. Zoback, *Tectonics* **8**, 237 (1989).
10. The 3-D velocity models determined for the Loma Prieta and Parkfield regions by other workers show good resemblance to our models where the regions studied overlap; this similarity demonstrates that the 3-D inversions of V_p are a stable process. For example, A. Michelini, W. Foxall, T. V. McEvilly, *Seismol. Res. Lett.* **61**, 48 (1990); A. Michelini and T. V. McEvilly, *Bull. Seismol. Soc. Am.* **81**, 524 (1991).
11. With 2-D and 3-D V_p models, respectively, R. L. Wesson [*Bull. Seismol. Soc. Am.* **61**, 729 (1971)] and C. H. Thurber (*5*) also found a sharp velocity discontinuity across the creeping section of the San Andreas fault.
12. P. Segall and R. Harris, *J. Geophys. Res.* **92**, 10,511 (1987). We plot the model shown in their figure 8B.
13. D. H. Oppenheimer, W. H. Bakun, A. G. Lindh, *ibid.* **95**, 8483 (1990).
14. M. Lisowski, W. H. Prescott, J. C. Savage, M. J. Johnston, *Geophys. Res. Lett.* **17**, 1437 (1990).
15. C. M. Poley, A. G. Lindh, W. H. Bakun, and S. S. Schulz [*Nature* **327**, 134 (1987)] showed that the Middle Mountain area had larger-than-usual strain response to the remote stress change from the Coalinga earthquake. This response might have been anticipated on the basis of the implied low rigidity and shear modulus of the low V_p material underlying Middle Mountain.
16. S. H. Hartzell and T. H. Heaton, *Bull. Seismol. Soc. Am.* **76**, 649 (1986).
17. G. Ekstrom, R. S. Stein, J. P. Eaton, D. Eberhart-Phillips, *J. Geophys. Res.*, in press; R. S. Stein and G. Ekstrom, in preparation.
18. J. R. Grasso [*Geophys. Res. Lett.* **10**, 229 (1983)] proposed that a high-velocity barrier marked the termination of an $M = 5.1$ event in the Pyrenees. As this is the size of some Loma Prieta aftershocks, this observation may agree with ours.
19. R. H. Sibson, *Bull. Seismol. Soc. Am.* **72**, 151 (1982).
20. M. R. J. Wyllie, A. R. Gregory, G. H. F. Gardner, *Geophysics* **23**, 459 (1958); T. Todd and G. Simmons, *J. Geophys. Res.* **77**, 3731 (1972); N. I. Christensen, *Geophys. J. R. Astron. Soc.* **79**, 411 (1984); D. Eberhart-Philips, D. Han, M. D. Zoback, *Geophysics* **82**, 82 (1989).
21. J. H. Dieterich, *Pure Appl. Geophys.* **116**, 790 (1978).
22. The material under Middle Mountain has low velocities and low resistivity, but normal gravity; these data suggest that the low velocities are caused by high pore pressures. This notion is also supported by the high V_P/V_S in this area (*10*). The spatial association of potentially high pore pressures with aseismic creep was suggested by W. P. Irwin and I. Barnes, *Geology* **3**, 713 (1975).
23. C. H. Scholz, *Bull. Seismol. Soc. Am.* **72**, 1 (1982).
24. J. C. Jaeger and N. G. W. Cook, *Fundamentals of Rock Mechanics* (Chapman and Hall, London, ed. 3, 1979), p. 354.
25. Working Group on California Earthquake Probabilities, *U.S. Geol. Surv. Open-File Rep. 88-398* (1988); D. P. Schwartz and R. H. Sibson, Eds., *ibid. 89-315* (1989).
26. G. King and J. Nabelek, *Science* **228**, 984 (1985).

27. We thank M. Blanpied, S. Hickman, D. Hill, A. Lindh, D. Oppenheimer, and two anonymous reviewers for thoughtful reviews of this manuscript.

4 February 1991; accepted 20 May 1991

$^{40}Ar/^{39}Ar$ Age of the Lathrop Wells Volcanic Center, Yucca Mountain, Nevada

BRENT D. TURRIN, DUANE CHAMPION, ROBERT J. FLECK

Paleomagnetic and $^{40}Ar/^{39}Ar$ analyses from the Lathrop Wells volcanic center, Nevada, indicate that two eruptive events have occurred there. The ages (136 ± 8 and 141 ± 9 thousand years ago) for these two events are analytically indistinguishable. The small angular difference (4.7°) between the paleomagnetic directions from these two events suggests they differ in age by only about 100 years. These ages are consistent with the chronology of the surficial geological units in the Yucca Mountain area. These results contradict earlier interpretations of the cinder-cone geomorphology and soil-profile data that suggest that at least five temporally discrete eruptive events occurred at Lathrop Wells approximately 20,000 years ago.

THE SOUTHWEST PART OF THE NEVADA Test Site (NTS) is being evaluated to determine its suitability for a high-level radioactive waste repository (*1–4*). Study of the chronology and eruptive volumes of lava from nearby volcanos are essential for assessing volcanic hazards during the mandated 10^4-year isolation period for the high-level radioactive waste.

Within the NTS, silicic volcanic activity produced several coalesced caldera complexes during the Miocene (14 to 8 million years ago) (*5, 6*). Since then, volcanism has been limited to small, isolated subalkaline to alkaline undersaturated basaltic volcanic centers (*7, 8*). The most recent volcanic activity at the NTS occurred at the Lathrop Wells volcanic center. A recent geomorphic and soil profile study suggested that at least five temporally discrete eruptive events occurred at Lathrop Wells at approximately 20 ka (thousand years ago) (*9*); these studies have large chronologic uncertainties and contradict radiometric and paleomagnetic data (*10*). We dated seven sites (Table 1) using the $^{40}Ar/^{39}Ar$ method to further evaluate the isotopic age of the Lathrop Wells volcanic center.

At the Lathrop Wells volcanic center,

B. D. Turrin, U.S. Geological Survey, 345 Middlefield Road, Menlo Park, CA 94025, and Institute of Human Origins, Geochronology Center, 2453 Ridge Road, Berkeley, CA 94709.
D. Champion and R. J. Fleck, U.S. Geological Survey, 345 Middlefield Road, Menlo Park, CA 94025.

flows of dense alkali olivine basalt with vesicular tops and bottoms, exhibiting block- and aa-flow morphologies, overlie Quaternary alluvium and Miocene ash flow and air-fall units of the Paintbrush Tuff. The basalt is sparsely porphyritic with olivine phenocrysts and plagioclase microphenocrysts (?) in a fine-grained groundmass of plagioclase, olivine, clinopyroxene (Ti-augite), opaque minerals (Fe-Ti oxides), interstitial glass, and apatite (*7, 8*). Hyalopilitic to pilotaxitic textures are common in some samples. The lava flows and scoria deposits locally contain xenoliths of the underlying Topopah Spring Member (?) of the Paintbrush Tuff [up to 0.03% by volume (*4, 11*)].

On the basis of the directions of remanent magnetization (*10*), field mapping, and geochronologic studies, two nearly synchronous eruptive events are identified at Lathrop Wells. The volcanic products from these events are spatially separated and are not in direct stratigraphic contact. We have inferred the following eruption history: (i) A northwest-trending fissure zone composed of local vents of irregular scoria mounds and agglutinate (unit Qs_5, Fig. 1), accompanied by eruption of small volume block and aa flows (unit Ql_5, Fig. 1). The later phases of this eruption produced the main scoria cone. (ii) Subsequently, volcanic activity occurred along a small, east-west fissure system, producing a lava flow unit (Ql_3, Fig. 1) that flowed to the east and south around the older flow and vent complex.

Three additional periods of volcanic activity have been suggested on the basis of cinder cone geomorphology and soil stratigraphic studies (*9, 12, 13*). Wells *et al.* (*9*) suggested that eolian and tephra deposits, which are adjacent to the main cinder cone and overlie the other volcanic units, represent three separate basaltic air-fall eruptions whose source is the main cinder cone. They suggest that these deposits have been modified by infilling with eolian material and

Table 1. $^{40}Ar/^{39}Ar$ age data from the Lathrop Wells volcanic center. Samples marked with an asterisk are considered contaminated and are not used. A, arithmetic mean; W, weighted mean; Comb., combined age of unit. Constants used in the age calculation are: $^{36}Ar_{Ca}/^{37}Ar_{Ca}$ = 0.000269; $^{39}Ar_{Ca}/^{37}Ar_{Ca}$ = 0.000729; $^{40}Ar_K/^{39}Ar_K$ = 0.002; J = 0.000125 [J is essentially the conversion factor of the $^{39}K(n,p)$ to ^{39}Ar reaction].

Sample	$^{40}Ar/^{39}Ar$	$^{37}Ar/^{39}Ar$	$^{36}Ar/^{39}Ar$	Age ± 1σ (ka)
Flow unit Ql_3				
1-86	40.939	1.741	0.137	143 ± 88
1-86	32.546	1.887	0.106	311 ± 78
1-86	98.908	1.821	0.334	66 ± 216
1-86	78.306	1.628	0.264	93 ± 212
A: 153 ± 110; SEM: ±55; W: 217 ± 54				
2-88	111.841	1.704	0.373	392 ± 215
2-88	105.308	1.776	0.354	194 ± 186
2-88	101.674	1.613	0.341	261 ± 232
2-88*	118.961	1.778	0.391	776 ± 162
A: 282 ± 101; SEM: ±58; W: 274 ± 120				
3-86	144.06	1.591	0.485	187 ± 243
3-86	200.13	1.723	0.676	110 ± 327
3-86	87.367	1.796	0.296	42 ± 185
3-86	50.708	1.827	0.170	145 ± 88
3-86	35.947	1.870	0.120	144 ± 84
3-86	49.092	1.940	0.165	126 ± 82
3-86*	6.756	0.315	0.009	947 ± 24
3-86*	47.030	1.855	0.153	452 ± 86
A: 126 ± 48; SEM: ±20; W: 133 ± 46				
4-86	12.901	1.868	0.042	172 ± 39
4-86	36.488	1.791	0.123	99 ± 196
4-86	13.417	1.726	0.043	211 ± 941
4-86	29.148	1.083	0.096	177 ± 212
4-86	24.048	1.083	0.080	147 ± 134
4-86	69.949	1.338	0.233	294 ± 379
4-86	42.058	0.830	0.141	112 ± 282
4-86*	28.660	1.894	0.091	450 ± 73
A: 173 ± 66; SEM: ±25; W: 187 ± 27				
Comb. Ql_3: A: 171 ± 87; SEM: ±20 W: 183 ± 21				
Flow unit Ql_5				
5-86	89.875	1.868	0.303	112 ± 90
5-86	116.184	1.805	0.392	107 ± 155
5-86	247.222	1.855	0.834	235 ± 521
5-86	82.812	1.772	0.277	228 ± 200
5-86	119.164	1.625	0.401	168 ± 318
5-86	71.786	1.791	0.244	−20 ± 263
5-86	221.233	1.419	0.744	368 ± 644
5-86	79.647	1.665	0.268	164 ± 89
A: 170 ± 114; SEM: ±40; W: 138 ± 54				
Scoria unit Qs_5				
223	132.604	1.600	0.449	7 ± 374
223	85.528	1.585	0.287	170 ± 180
223	66.262	1.659	0.222	151 ± 197
223	82.477	1.532	0.276	228 ± 165
A: 139 ± 94; SEM: ±47; W: 175 ± 100				
211	28.492	1.311	0.095	139 ± 81
211	56.991	1.154	0.190	182 ± 125
211	164.499	1.425	0.557	20 ± 285
211	46.959	1.337	0.157	138 ± 80
A: 120 ± 70; SEM: ±35; W: 142 ± 51				
Comb. Qs_5: A: 129 ± 77; SEM: ±27 W: 149 ± 45				
Comb. Qs_5 + Ql_5: A: 150 ± 96; SEM: ±24 W: 144 ± 35				

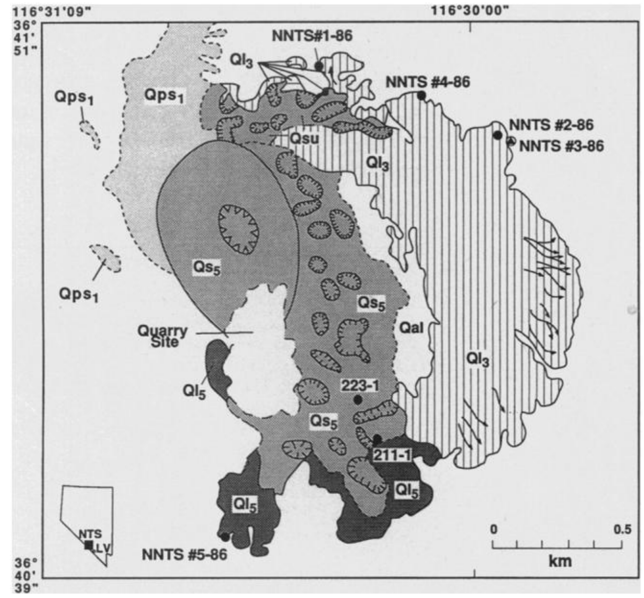

Fig. 1. Generalized geologic map of the Lathrop Wells cinder cone and flow complex, showing locations of sampling sites for $^{40}Ar/^{39}Ar$ analyses. Numbers correspond to samples listed in Table 1. Areas enclosed with hachured outlines are scoria mounds composed of welded agglutinate and volcanic bombs; area enclosed with saw-toothed outline is crater at top of main scoria cone. Units: Ql_3, late basaltic lava flows; Ql_5, early scoria deposits; Qps_1, pyroclastic base-surge deposits; Qsu, undifferentiated scoria deposits, with some scoria mounts contemporaneous with unit Ql_3. Unpatterned areas, Quaternary alluvium.

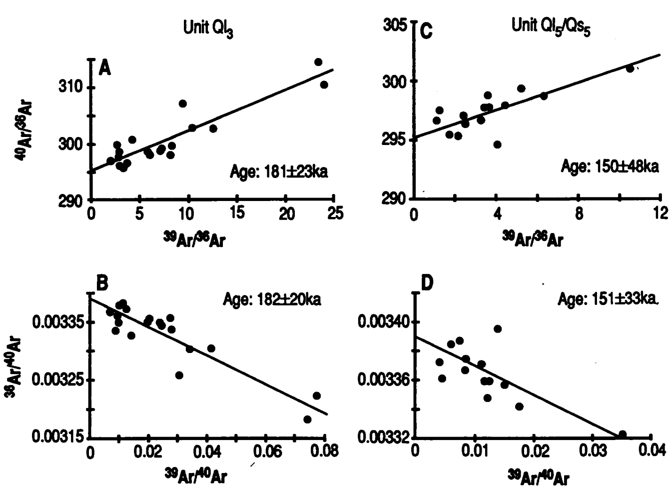

Fig. 2. Isochron and inverse-isochron plots for unit Ql_3 and (composite) unit Ql_5/Qs_5. Isochron and inverse-isochron plots for unit Ql_3 show an age of 181 ± 23 and 182 ± 20 ka, respectively, and an initial $^{40}Ar/^{36}Ar$ intercept of 295.3 ± 0.5 with a mean square of the weighted deviates (MSWD) of 0.96. Isochron and inverse-isochron plots for composite unit Ql_5/Qs_5 show ages of 150 ± 48 and 151 ± 33 ka, respectively, and an initial $^{40}Ar/^{36}Ar$ intercept of 295.1 ± 0.7 with a MSWD of 0.75. The MSWD for each regression is less than 1, suggesting that the errors about the regression lines may be attributable solely to analytical errors in individual isotopic measurements.

formation of several soil profiles. Wells *et al.* (*9*) concluded that these eruptive events occurred approximately 20 ka or younger, "as much as an order of magnitude" younger than "previous (K-Ar) age determinations" for the Lathrop Wells volcanic center.

To evalute this history, we obtained 40 $^{40}Ar/^{39}Ar$ ages on samples from the Lathrop Wells volcanic center. All of the $^{40}Ar/^{39}Ar$ analyses are from the total fusion of individual whole-rock grains, 0.3 to 0.5 mm in size (*14*). The samples yielded a weighted average (*15*) of 183 ± 21 ka for unit Ql_3, 138 ± 54 ka for unit Ql_5, and 149 ± 45 ka for unit Qs_5 (Table 1). Isochron and inverse-isochron ages are concordant with the weighted mean ages (Fig. 2). These $^{40}Ar/^{39}Ar$ ages are concordant with the published K-Ar ages of 116 ± 13 and 133 ± 10 ka for unit Ql_5 and unit Ql_3, respectively (*10*). Isochron data on samples from the lavas at Lathrop Wells indicate an initial $^{40}Ar/^{36}Ar$ ratio equivalent to atmospheric Ar (*16*). This

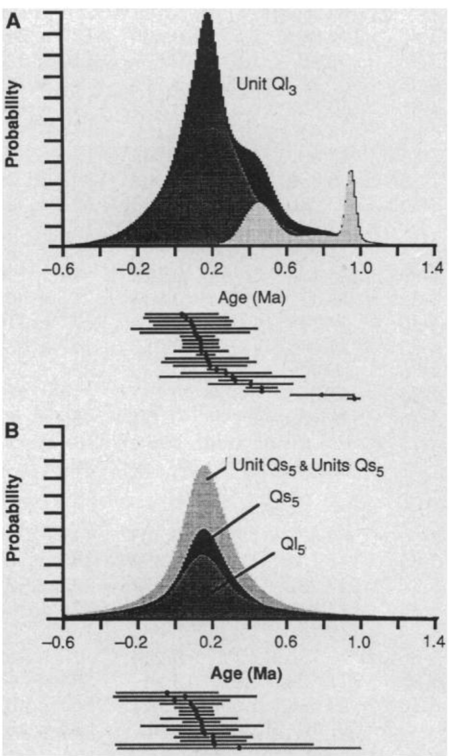

Fig. 3. Ideograms showing integrated probability distributions of $^{40}Ar/^{39}Ar$ ages. Individual analyses are shown as single points with 2σ error bars. (**A**) Unit Ql_3—light gray areas, integrated probability distribution of contaminated samples; dark gray areas, integrated probability distribution of uncontaminated samples; black areas, integrated probability distribution of all unit Ql_3 samples. (**B**) Units Ql_5 and Qs_5—light gray areas, integrated probability distribution of all samples from units Ql_5 and Qs_5; dark gray areas, integrated probability distribution of all samples from unit Ql_5; black areas, integrated probability distribution of all samples from unit Ql_3. Ma, million years ago.

result shows that excess ^{40}Ar is not present homogeneously throughout the lavas.

There is some evidence of xenolith contamination of the Ql_3 flow from the underlying rhyolite tuffs. The contaminated samples yield distinctly older ages (Fig. 3 and Table 1). A 0.03% contamination of the basalt by the underlying tuff would add an additional 0.022 million years to the age of the Lathrop Wells flow (*10*).

Directions of remanent magnetization of the eruptive products from the Lathrop Wells center (*10*) form two groups, which correlate with units Qs_5 and Ql_3. A statistical comparison of the mean directions for units Qs_5 and Ql_3 (51.5° inclination, 2.2° declination, and 51.5° inclination, 354.6° declination) shows that they differ at the $P = 0.0002$ significance level (*17*). The time interval between these two directions of magnetization cannot be determined uniquely from paleomagnetic data alone. On the basis of paleomagnetic and chronologic studies of Sunset Crater in Arizona (*18*), the angular difference of 4.7° suggests that the age difference between the two eruptive events is about 100 years.

A single site consisting of 40 core samples from bedded volcanic bombs from the rim of the main cinder cone has a direction of remanent magnetization identical to that of unit Qs_5. There is no evidence of any unconformity or stratigraphic contact between the scoria deposits of the main cinder cone and the agglutinate and scoria deposits of unit Qs_5. The relations indicate that there was no time break between deposition of these units and that the main cinder cone, irregular scoria mounds, and agglutinate of units Qs_5 are a single unit. Units Ql_5 and Qs_5 (including the main cinder cone) are thus flow and vent facies of a single eruptive event. The weighted average of the combined $^{40}Ar/^{39}Ar$ ages from units Ql_5 and Qs_5 is 144 ± 35 ka. The best estimate for the age of this event is given by the combined weighted mean ages of all the available K-Ar (*10*) and $^{40}Ar/^{39}Ar$ radiometric ages from Qs_5 and Ql_5, and is 136 ± 8 ka.

The best estimate for the age of unit Ql_3 is the weighted mean of all the available radiometric ages, which is 141 ± 9 ka. From the reported analytical precision of the combined weighted mean ages for Ql_3 and (composite) unit Qs_5-Ql_5, the absolute age difference between these units is, at most, 29 ka (*19*).

The age estimates for the Lathrop Wells volcanic center are corroborated by two U-Th ages on massive laminated stalactitic calcrete from beneath the unit Ql_3 lava flow that are 345 (+80/−70) and 345 (+180/−71) ka (*20*). A third U-Th age, obtained on carbonate at the base of the eolian sand and silt and tephra (?) deposits is 25 ± 10 ka (*20*). This younger age is a minimum because this type of pedogenic carbonate may not necessarily be a closed system with respect to uranium (*21*). Moreover, some time is required between the eruption of a lava flow and the accumulation of eolian material and the formation of pedogenic carbonate. The U-Th age on calcrete from beneath unit Ql_3 requires that the unit Ql_3 flow be younger than 345 (+180/−70) ka and older than 25 ± 10 ka. In addition, tighter age control is provided by alluvial deposits 3 to 4 km northwest of Lathrop Wells that contain primary and reworked cinders thought to have come from the Lathrop Wells volcanic center. Uranium trend dates on the Quaternary stratigraphic units in the Yucca Mountain area (*22*) indicate that the cinders were deposited between 240 ± 30 and 145 ± 25 ka.

The reported isotopic ages and independent geologic evidence contradict recent interpretations of cinder cone geomorphology and soil profile data (*9*) that suggest that there were at least five temporally discrete eruptive events at Lathrop Wells, at an age of approximately 20 ka. This age estimate, based on geomorphic and soil profile data, which are, at best, semiquantitative and more likely qualitative, is miscalibrated.

REFERENCES AND NOTES

1. G. L. Dixon *et al.*, *Geol. Soc. Am.* **12**, 409 (1980).
2. *Site Characterization Plan, Yucca Mountain Site, Nevada, Research and Developments Area, Nevada* (*Rep. DOEIRW-0199*, U.S. Department of Energy, Office of Civilian Waste Management, 1988), vol. 1, part A, chaps. 1 and 2.
3. B. M. Crowe and W. J. Carr, *U.S. Geol. Surv. Open-File Rep. 80-357* (1980).
4. B. M. Crowe *et al.*, *J. Geol.* **91**, 259 (1983).
5. F. M. Byers *et al.*, *U.S. Geol. Surv. Prof. Pap. 919* (1976).
6. R. L. Christensen *et al.*, *Geol. Soc. Am. Bull.* **88**, 943 (1977).
7. D. T. Vaniman and B. M. Crowe, *Los Alamos Natl. Lab. Rep. LA-8845-MS* (1981).
8. D. T. Vaniman *et al.*, *Contrib. Mineral Petrol.* **80**, 341 (1982).
9. S. G. Wells *et al.*, *Geology* **18**, 549 (1990).
10. B. D. Turrin *et al.*, *U.S. Geol. Surv. Bull.*, in press.
11. This equates to 0.064% tuff xenoliths by volume (0.058% by weight) for the Lathrop Wells lava flows, for densities of 1.5 g/cm^3, 3.0 g/cm^3, and 2.7 g/cm^3 for the scoria, lava flows, and tuff, respectively.
12. C. E. Renault *et al.*, *Geol. Soc. Am. Abstr. Prog.* **20**, A115 (1988).
13. S. G. Wells *et al.*, *ibid.*, p. A242 (1988).
14. Argon extractions and isotopic analyses were conducted at the Institute of Human Origins, Geochronology Center, with a fully automated $^{40}Ar/^{39}Ar$ laser fusion–microextraction system. This extraction system is in-line with a Mass Analyzer Products MAP 215 mass spectrometer, operated at a 500 to 600 resolution. Argon backgrounds for this instrument are typically: $^{40}Ar \le 2.0 \times 10^{-12}$ cm^3 (STP); $^{39}Ar \le 5.0 \times 10^{-14}$ cm^3 (STP); $^{37}Ar \le 7.0 \times 10^{-14}$ cm^3 (STP); $^{36}Ar \le 2.0 \times 10^{-14}$ cm^3 (STP). The detection limit is on the order of 1.0×10^{-14} cm^3 (STP). Samples of whole-rock basalt were crushed or sliced to 0.5 to 1 cm. Fragments were then examined for xenolithic contamination. Contamination-free chips were crushed further, sieved (60 to 100 mesh), and washed. The samples were then treated with a 10% HCl solution and a 5% HF

solution in an ultrasonic bath for 10 and 5 min, respectively, and then rinsed in distilled water in an ultrasonic bath for 5 min. From this material, approximately 250 whole-rock grains were picked for irradiation. Samples for irradiation were encapsulated in aluminum cups and arranged in a known geometry along with mineral standards. The sample package was placed in a cadmium lined, 2.5-cm-diameter aluminum tube. Then the sample set was irradiated 10 min at 8 MW in the hydraulic rabbit of the Los Alamos National Laboratory Omega West reactor by fast neutrons to produce the reaction $^{39}K(n,p)$ ^{39}Ar. After irradiation, the samples were transferred to a copper sample holder and loaded into the Ar-extraction system. Fusion was induced by a 6-W continuous Ar-ion laser beam focused to a 2- to 3-mm spot, applied for 30 to 60 s. The gases released from the grains were then scrubbed for reactive species (CO_2, CO, and N_2) by exposure to a 150°C Zr-Fe-V alloy getter for 3 to 5 min. The remaining inert gases, principally Ar, were then admitted to the mass spectrometer, and the argon-isotopic ratios were determined. The mass spectrometer was operated in static mode with the use of automated data-collection procedures. The age is then calculated from the $^{40}Ar/^{39}Ar$ ratio after all interfering Ar-isotopes from atmospheric contamination and undesirable neutron reactions with Ca and K are corrected [N. R. Brereton, *Earth Planet. Sci. Lett.* **8**, 427 (1971); G. B. Dalrymple and M. A. Lanphere, *ibid.* **12**, 300 (1971)].

15. J. R. Taylor, *An Introduction of Error Analysis, the Study of Uncertainties in Physical Measurements* (Oxford Univ. Press, New York, 1982). Weighted means, in the tables, are calculated by multiplying the individual analyses by 1 over the variance. The uncertainty of the weighted average is obtained by pooling the variances. The preferred age given for any set of data is the weighted average because the more precise analyses are given more weight in the determination of the average age.
16. The $^{40}Ar/^{36}Ar$ ratio of atmospheric Ar is 295.
17. P. L. McFadden and D. L. Jones, *Geophys. J. R. Astron. Soc.* **67**, 53 (1981).
18. The geomagnetic field is not constant in direction or intensity at any given location through time, but instead undergoes a secular variation at a rate of about 4° per century [D. E. Champion and E. M. Shoemaker, *NASA Tech. Mem. 78,436* (1977), p. 7; D. E. Champion, *U.S. Geol. Surv. Open-File Rep. 80-824* (1980)].
19. This value (0.029 million years ago) is the minimum difference in age between the two flows that is detectable at the 95% confidence level. See p. 120 of G. B. Dalrymple and M. A. Lanphere, [*Potassium-Argon Dating* (Freeman, San Francisco, 1969)].
20. B. J. Szabo *et al.*, *U.S. Geol. Surv. Open-File Rep. 81-119* (1981).
21. The principal source of error in U-Th dating lies in the assumption of a closed system [G. H. Curtis, *U.S. Nucl. Reg. Comm. Rep. NUREG/CR-2382* (1981)]. It has been shown that U-Th dates on soil carbonates from soils formed on K-Ar dated basaltic lava flows were consistently younger than the K-Ar dates by up to an order of magnitude [J. L. Slate, thesis, University of Arizona (1985)].
22. W. C. Swadley *et al.*, *U.S. Geol. Surv. Open-File Rep. 84-788* (1984).
23. The manuscript was improved by comments by G. B. Dalrymple, M. A. Lamphere, D. Noble, E. H. McKee, and J. C. Dohrenwend.

22 January 1991; accepted 3 June 1991

A Novel, Highly Stable Fold of the Immunoglobulin Binding Domain of Streptococcal Protein G

ANGELA M. GRONENBORN,* DAVID R. FILPULA, NINA Z. ESSIG, ANIRUDDHA ACHARI, MARC WHITLOW, PAUL T. WINGFIELD, G. MARIUS CLORE*

The high-resolution three-dimensional structure of a single immunoglobulin binding domain (B1, which comprises 56 residues including the NH_2-terminal Met) of protein G from group G *Streptococcus* has been determined in solution by nuclear magnetic resonance spectroscopy on the basis of 1058 experimental restraints. The average atomic root-mean-square distribution about the mean coordinate positions is 0.27 angstrom (Å) for the backbone atoms, 0.65 Å for all atoms, and 0.39 Å for atoms excluding disordered surface side chains. The structure has no disulfide bridges and is composed of a four-stranded β sheet, on top of which lies a long helix. The central two strands (β1 and β4), comprising the NH_2- and COOH-termini, are parallel, and the outer two strands (β2 and β3) are connected by the helix in a +3*x* crossover. This novel topology (−1, +3*x*, −1), coupled with an extensive hydrogen-bonding network and a tightly packed and buried hydrophobic core, is probably responsible for the extreme thermal stability of this small domain (reversible melting at 87°C).

PROTEIN G IS A LARGE MULTIDOMAIN cell surface protein of group G *Streptococcus*, which is thought to help the organism evade the host defenses through its protein binding properties (*1*). A repeating 55-residue domain binds to the F_c region of immunoglobulin G (IgG) and to α2-macroglobulin, a major protease inhibitor of human plasma (*1*). There are two such repeats in protein G from strain GX7809 and three for the protein from strain GX7805, and the sequence identity between the various repeats is greater than 90% (*1*). Microcalorimetry of one of these domains, known as B1 (*2*), reveals extreme thermal stability with a melting temperature (T_m) of 87°C and completely reversible thermal denaturation (*3*). Further, the unfolding transition on urea gradient gel electrophoresis (*4*) cannot be observed in full as the protein remains native up to ~8 M urea. These features are highly unusual considering the small size of the domain and the absence of any disulfide bridges or tightly bound prosthetic group. For comparison, the average T_m in a recent compilation of the thermodynamic parameters of unfolding for a large number of proteins is ~63°C, and only three proteins in this collection are more stable than the B1 domain, namely, the Ca^{2+} bound form of parvalbumin (90°C), neurotoxin II (96°C), and bovine pancreatic trypsin inhibitor (BPTI) (100°C) (*5*). The potential importance of the B1 domain of protein G as an analytical tool in immunology, together with its extreme physicochemical properties, prompted us to undertake the determination of its three-dimensional (3D) structure in solution by NMR (*6*) spectroscopy.

The ^1H-NMR spectrum of the B1 domain was assigned by using conventional 2D NMR methodology (*7*) on a Bruker AM600 spectrometer. Spin systems were delineated by using PE.COSY (*8*) and HOHAHA (*9*) spectroscopy to demonstrate direct and relayed through-bond connectivities, respectively, while NOESY (*10*) spectroscopy was used to identify through-space (<5 Å) interactions. The assignment was slightly more complex than expected because of the duplication of the resonances for 22 residues arising from the presence of two species in a ~3:7 mixture with and without post-translational processing of the NH_2-terminal Met, respectively. The pattern and relative intensities of the NOEs for the two species, however, were the same within experimental error. Approximate interproton distance restraints were obtained from NOESY spectra recorded at mixing times of 50, 100, and 150 ms, and grouped into three classes, 1.8 to 2.7 Å, 1.8 to 3.3 Å (1.8 to 3.5 Å for distances involving NH protons), and 1.8 to 5.0 Å, which correspond to strong, medium, and weak NOEs, respectively (*11, 12*). To help resolve ambiguities in NOE assignments, spectra were recorded at 25° and 41°C. The $^3J_{HN\alpha}$ and $^3J_{\alpha\beta}$ coupling constants were measured from PE.COSY spectra. Stereospecific assignments and ϕ, ψ, and χ1 torsion angle restraints were obtained

A. M. Gronenborn and G. M. Clore, Laboratory of Chemical Physics, Building 2, National Institute of Diabetes and Digestive and Kidney Diseases, National Institutes of Health, Bethesda, MD 20892.
D. R. Filpula, N. Z. Essig, A. Achari, M. Whitlow, Genex Corporation, 16020 Industrial Drive, Gaithersburg, MD 20877.
P. T. Wingfield, Protein Expression Laboratory, Building 6, Office of the Director, National Institutes of Health, Bethesda, MD 20892.

*To whom correspondence should be addressed.